

The alterations of brain effective connectivity in major depressive disorder through multisite rs-fMRI data

Peishan Dai^{a*}, Yun Shi^a, Tong Xiong^a, Xiaoyan Zhou^a, Shenghui Liao^a, Zhongchao Huang^b, and the REST-meta-MDD Consortium

^aSchool of Computer Science and Engineering, Central South University, Changsha, Hunan, China.

^bDepartment of Biomedical Engineering, School of Basic Medical Science, Central South University, Changsha, Hunan, China

Email: [*daipeishan@csu.edu.cn](mailto:daipeishan@csu.edu.cn)

Keywords: Major Depressive Disorder; Effective Connectivity; Machine Learning; Feature Selection; Granger Causality Analysis

Abstract

The current diagnosis of major depressive disorder (MDD) primarily relies on the patient's self-reported symptoms and a clinical evaluation. The functional connectivity (FC) feature of resting-state functional magnetic resonance imaging (rs-fMRI) is widely used for the classification of MDD. However, the performance of FC features on the large-scale cross-site dataset is not good enough, which is a bottleneck in the application of classification methods in the clinical diagnosis of MDD. As it can reflect the directed connections between brain regions compared to FC, effective connectivity (EC) has the potential to improve the classification performance on large-scale, multi-site MDD datasets. Granger causality analysis was used to extract EC from a large multi-site MDD dataset. ComBat algorithm and multivariate linear regression were used to harmonize site difference and to remove age and sex covariates, respectively. Two-sample t-test and model-based feature selection methods were used to screen highly discriminative EC for MDD. At last, LightGBM was used to classify MDD. In the REST-Meta-MDD Consortium dataset, 97 EC with highly discriminative for MDD were screened. In the nested five-fold cross-validation, the best classification model using 97 EC achieved the accuracy, sensitivity, and specificity of 94.35%, 93.52%, and 95.25%, respectively. In the DecNef Project Brain

Data Repository dataset, which tests the generalization performance of 97 EC, the best classification models achieved 94.74%, 90.59%, and 96.75% accuracy, sensitivity, and specificity, respectively.

Introduction

Major depressive disorder (MDD) is a common mental illness that severely impacts a person's quality of life. Currently, the diagnosis of MDD is mainly based on the patient's self-report and mental state examination, which cannot reflect the patient's brain activity characteristics and, to some extent, will affect the diagnosis and treatment of the disease^[1,2,3,4]. Due to the ability of non-invasive observing human brain activity, resting-state functional magnetic resonance imaging (rs-fMRI) is increasingly used for the classification of MDD^[5,6].

In current rs-fMRI-based MDD classification research, Functional connectivity (FC) is the most commonly used classification feature. FC uses Pearson correlation to calculate the correlation between two brain regions, which represents how different brain areas communicate and work together to perform various cognitive and emotional processes. Previous studies have shown that MDD patients have abnormal FC compared to healthy control (HC) groups^[7,8], indicating that FC is an effective feature for MDD research. FC is widely used in the classification of various mental illnesses, including MDD. Research in this area has yielded a significant amount of findings^[9,10,11]. However, in the current FC applied to MDD classification studies, the sample size of most studies is relatively small, the generalizability of the classification model needs further validation, and the classification performance is not sufficient to apply the related classification methods to the clinical diagnosis of MDD^[12,13,14,15]. FC is non-directional and cannot reflect the direction of information transfer between brain regions, it only reflects the strength of correlation between two brain regions. Therefore, applying FC to classify psychiatric disorders including MDD may be difficult to achieve high classification performance.

Effective connectivity (EC) refers to the causal interactions between different brain regions, meaning how one brain region influences the activity of another^[16]. It is used to study the direction and strength of these interactions and how they contribute to the implementation of cognitive and emotional

processes. EC can be distinguished from FC which refers to the temporal correlations between brain regions, without necessarily implying causality. EC can be inferred using techniques such as Granger causality analysis (GCA) and dynamic causal modeling (DCM). GCA can be used to infer the causal relationship between time series data, such as neural activity recorded from different brain regions^[17,18].

Currently, GCA-based EC has been widely used in fMRI studies to reveal causal relationships between brain regions^[19,20,21]. Liu et al. found that the EC between the right ventrolateral prefrontal cortex and the left temporal-parietal junction in the ventral attention network is related to depression²². Many studies have also found multiple EC associated with depression^[23,24,25]. However, to our knowledge, there are relatively few studies applying EC to classify the effects of mental disorders, including MDD, and the sample sizes of related studies are relatively small. Geng et al. obtained good classification results by using only the EC extracted from the default mode network (DMN), dorsal attention network (DAN), frontal-parietal network (FPN), and salience network (SN) on a small sample dataset²⁶.

Geng et al.'s research suggests that both FC and EC show potential for identifying MDD, but EC may be more effective compared to FC²⁶. Additionally, Geng et al.'s research selected a small number of EC between networks, whereas utilizing whole-brain EC and data feature selection methods to select features may further improve classification performance.

In this study, we use GCA to extract EC from the large sample, cross-site MDD dataset " REST-meta-MDD Consortium". Through feature selection methods, we select features with significant discriminative ability, and use machine learning classifiers to classify depressed and healthy subjects. We also try to mine for EC biological markers for MDD.

Results

Comparison of classification performance of different classification models. We compared the classification performance of the LightGBM²⁷ model we used with that of commonly used machine learning and deep learning methods. To ensure comparability, all EC experiments used the 13340 EC

in the EC matrix, all FC experiments used the 6670 FC in the FC matrix. The results of the experiments are shown in [Table 1](#). From Table 1, it can be seen that the LightGBM classification method used by us is better than the traditional machine learning methods Rbf-SVM, Random Forest, and XGBoost²⁸. Our classification method is also better than the currently popular deep learning classification methods, GCN²⁹, BrainNetCNN³⁰, and Transformer³¹. Additionally, it is observed that models trained with EC generally outperform those trained with FC. This trend is evident across experimental results. The comparison of the ROC curve of machine learning and deep learning models is shown in Supplementary Figure S1.

Table 1. The comparison of the classification performance of machine learning and deep learning models.

The impact of feature selection on the classification performance. In the feature selection procedure, we used both SVM-RFECV implemented by Scikit-learn³² and LightGBM for feature selection, but the SVM-RFECV selected fewer EC features. Therefore, we used LightGBM's "feature_importances_" function to select important features, which are taken as features highly discriminative for MDD, for training LinearSVM and LightGBM models. The comparison of the classification performance of LinearSVM and LightGBM classifiers before and after feature selection is shown in [Table 2](#). As can be seen from Table 2, after feature selection, the number of EC decreased from 13340 to 97, greatly reducing the dimension of the features. After feature selection, both the LinearSVM and LightGBM classification models had significantly improved classification performance. We can see that the LightGBM model that uses feature-selected EC obtains the best classification results, achieving the accuracy, sensitivity, and specificity of 94.35%, 93.52%, and 95.25%. The ROC curve of two classifiers before and after feature selection is shown in Supplementary Figure S2.

Table 2. The classification performance of two classifiers before and after feature selection.

Migration experiments of the highly discriminative EC selected by our study. To test whether our extracted highly discriminative EC have good generalization performance, we use the dataset from DecNef Project Brain Data Repository (<https://bicr-resource.atr.jp/srpbsoopen/>) to test the generalization

performance of these features. As shown in [Table 3](#), the 97 highly discriminative EC we extracted showed excellent classification performance on the DecNef Project Brain Data Repository dataset, indicating some generalization ability. The ROC curve of migration experiments with highly discriminatory EC is shown in Supplementary Figure S3.

Table 3. The results of migration experiments with highly discriminatory EC.

Comparison of the results of the proposed method with other studies using FC or EC features for MDD classification. [Table 4](#) shows a comparison of recent research results on classifying MDD using FC or EC features. It can be seen that our method achieved the best classification results by using the largest sample size. It can also be seen that most of the current MDD classification studies primarily use FC features. There are also studies that use EC for MDD classification (Geng et al.²⁶), but the sample size is small and the classification performance of the study was also lower than that of our method.

In our previous research (Table 4, Dai et al.⁸), we used the same dataset as this study to mine important FC and network attribute features, and obtained 68.90% classification performance in the five-fold cross-validation scenario. However, if we only use FC, we can only achieve 67.10% classification performance. This suggests that using large-scale, cross-site rs-fMRI data for the accurate classification of MDD is highly challenging. However, we achieved a 94.35% classification accuracy using EC features in this study, which significantly improved the classification performance for MDD. This is consistent with Geng et al.'s study, which found that EC is more effective than FC in identifying MDD, and it indicates that EC has a stronger discrimination ability for MDD than FC.

Table 4. The comparison of recent research results on classifying MDD using FC or EC features.

Contribution analysis of important features. We used SHAP to assign the contribution of each feature to the best classification model. As we used nested five-fold cross-validation to train and test the classification model, we used SHAP to assign the contribution of features to the model on each fold of the five-fold cross-validation (outer loop). One of the feature contribution assignment results is

shown in [Figure 4](#). We provide all results of the feature contribution assignment in Supplementary Material (see Supplementary Figure S4-S8).

Figure 4. Analysis of the contribution of important features.

We obtained five results of feature contribution assignment in the nested five-fold cross-validation procedure. In [Table 5](#), we counted the EC features with a number of occurrences greater than or equal to 3 for the five results.

Table 5. High-contributing EC

Based on the data presented in Table 5, a visualization of the brain was generated using BrainNet Viewer³⁹, as depicted in the following [Figure 5](#).

Figure 5. Brain visualization of high-contributing EC.

We used LightGBM to extract 97 EC that have excellent discrimination ability. It is worth noting that EC that originate from the cerebellum make up the majority, particularly the 107th ROI-Cerebellum_10_L and 102nd ROI-Cerebellum_7b_R in AAL.

The details of the 97 highly discriminative EC for MDD we selected are provided in Supplementary Material (see Supplementary Table S4).

Discussion

In this study, we extracted EC from 116 brain regions across the entire brain, achieving high-precision classification between MDD and HC groups in a cross-site, large-sample dataset. We have mined EC that are highly discriminative for MDD. The results of our classification model on the large-sample dataset set a new benchmark for performance in this field.

The classification effects of FC and EC. Our experimental results indicate that, in classifying MDD based on rs-fMRI data, EC has superior performance compared to FC. Additionally, research on MDD classification using EC is less common than research using FC, but EC has achieved good classification results. Geng et al.'s research, although using a smaller sample (24 MDDs: 24 HCs), also

showed that EC has a stronger MDD recognition ability compared to FC. Our research results may suggest that EC, which can obtain directional information, has more rich information than FC, which only obtains correlation information, and can help improve the performance of classifiers.

Achieving high classification performance on the large-scale, cross-site dataset of MDD is the foundation for truly applying models to MDD clinical diagnosis. As a result, a large number of studies currently focus on using FC to classify MDD, while we have achieved classification performance that far surpasses that of FC using EC. Our research results are expected to significantly improve the classification performance of large-scale, cross-site MDD datasets, and have the potential to truly apply classification models to assist in the clinical diagnosis of MDD patients, and can also be extended to the analysis of disease subtypes and differences in drug treatment. In addition, our initial experiments on other basic data also indicate that this method has the potential to be extended to the analysis of other mental illnesses, and related research results will be reported in future studies.

The alterations of brain EC in MDD. The resting-state networks distinct at rest have been confirmed in many studies^[40,41], which mainly include the default mode network (DMN), visual network (VN), sensorimotor network (SMN), attention network (AN), salience network (SN) and frontal-parietal network (FPN)²⁶. Our research showed that the number of EC across the networks is significantly higher than the number of EC within the networks, which may indicate that MDD has a stronger impact on inter-network EC than that on intra-network.

We found that MDD may alter EC between some brain regions, particularly in cerebellar regions. In the EC that we screened, those with cerebellar regions as the starting point accounted for the majority. These were mainly concentrated in the Cerebellum_7b_R and Cerebellum_10_L. The cerebellum is not only involved in motor function, but also related to various higher-order functions, including cognition and emotion^[42,43,44], fear memory⁴⁵, emotional processing⁴⁶, etc. Increasingly studies have shown the role of the cerebellum in emotional and social cognition. Abnormalities in cerebellar structure and functional connectivity have been found in several main psychiatric disorders (bipolar disorder,

schizophrenia, generalized anxiety disorder, obsessive-compulsive disorder, severe depression, etc.)⁴⁷.

Many studies have also found abnormalities in cerebellar structure and function in MDD patients^[24,48].

The changes in EC found in our study of MDD patients also indicate that changes in cerebellar function are closely related to MDD.

Main conclusions. We explored the alterations of brain EC in MDD based on a large cross-site rs-fMRI dataset. The main findings can be drawn from this work as follows: 1. EC has a better discriminative ability for MDD than FC. The MDD classification model we established has significantly better performance than other large cross-site MDD classification studies. It also has great potential for other psychiatric rs-fMRI datasets. Our research has the potential to drive the application of psychiatric disease classification, including MDD, in clinical diagnosis. 2. High-discriminative EC are mainly concentrated in the cerebellum, and most of them start from the cerebellum, which may indicate that the information transfer from the cerebellum to other brain regions is closely related to MDD. This may reveal the need to further investigate the relationship between EC of the cerebellum to cerebral regions and MDD. 3. Regardless of whether it is FC or EC, cross-network connections are significantly higher than intra-network connections. This deepens our understanding of the brain function of MDD patients.

Limitations and prospects. 1. This study only used EC features for the classification of MDD, and combining FC and other features may further improve classification performance. 2. The samples used in this study were from China, and population distribution may differ between countries, which may affect the results of the analysis. In future studies, we will include other racial groups' rs-fMRI data samples. 3. This study focused only on the classification of MDD, and in the future, the method will be extended to the classification of other large cross-site psychiatric disease imaging.

Methods

Participants. In our study, we built and tested the classification model using the REST-Meta-MDD Consortium (<http://rfmri.org/REST-meta-MDD>), a cross-site large sample dataset of Chinese people, and extracted MDD-altered EC. The extracted MDD-altered EC were then used to test the generalization performance in the DecNef Project Brain Data Repository (<https://bicc-resource.atr.jp/srpbsopen/>), a cross-site large sample dataset of Japanese people.

The REST-Meta-MDD Consortium dataset for extracting MDD-altered EC. The dataset used in this research was collected by the REST-Meta-MDD Consortium. This dataset consists of 1300 MDDs and 1128 HCs from 25 sites⁴⁹. In order to ensure the quality of the data, we followed the steps shown in [Figure 1](#) for data selection. We added the sample discarding step into the data screening process of Yan et al. to exclude the samples with some missing ROIs signals.). As a result, 832 MDDs and 779 HCs from 17 sites were used in this study.

Figure 1. Sample screening procedure.

The demographic information of all participants is summarized in Supplementary Material (see Supplementary Table S1).

The DecNef Project Brain Data Repository dataset for testing the generalization performance of extracted MDD-altered EC. Data used in the preparation of this work were obtained from the DecNef Project Brain Data Repository (<https://bicc-resource.atr.jp/srpbsopen/>) gathered by a consortium as part of the Japanese Strategic Research Program for the Promotion of Brain Science (SRPBS) supported by the Japanese Advanced Research and Development Programs for Medical Innovation (AMED). The demographic information of all participants is summarized in Supplementary Material (see Supplementary Table S2).

Data Preprocessing. The DPARSF software⁵⁰ was used to preprocess the data (<http://www.rfmri.org/DPARSF>). The steps include: (1) Discarding the first ten volumes of the rs-fMRI data to eliminate the effects of magnetic field instability (2) Applying slice-time correction and realigning the image using a six-parameter (rigid body) linear transformation. (3) Co-registering the

T1-weighted images to the mean functional image using a six degrees-of-freedom linear transformation without re-sampling. (4) Segmenting the T1-weighted images into gray matter (GM), white matter (WM), and cerebrospinal fluid (CSF). (5) Normalizing all images to the MNI space. (6) Regressing head motion effects using the Friston 24-parameter model⁵¹. (7) Filtering all the time series using a temporal bandpass filter (0.01~0.1Hz).

EC extraction. The rs-fMRI data were first preprocessed, and then the automated anatomical labeling (AAL) atlas was utilized to parcellate the entire brain into 116 regions⁵². The time-series of each of the 116 brain regions were obtained by averaging the time-series of all the voxels within the brain region.

We used the REST-GCA software to perform EC calculations based on the signed path coefficient algorithm¹⁸. REST-GCA utilizes a Granger causality relationship model to calculate the EC between time-series representing the activity of different brain regions. The positive/negative sign of the path coefficient indicates that the activity of one brain region can respectively predict an increase/decrease in the activity of another brain region. This increase/decrease may indicate an excitatory/inhibitory effect of one brain region on another. The magnitude of the EC represents the strength of directed connections between different brain regions.

The GCA model was used to calculate the EC between each pair of the 116 time-series extracted using the AAL atlas. We obtain one EC matrix with the dimension of 116*116, including two EC for a pair of time series: the EC from brain area x to brain area y, and the EC from brain area y to brain area x, corresponding to the upper right and lower left triangles of the matrix respectively.

Site variance harmonization and biological covariate suppression. To reduce the effect of site differences on classification performance, the ComBat algorithm (https://github.com/Warvito/neurocombat_sklearn) was used to harmonize site differences^[53,54,55]. To reduce the effect of biological covariates on classification performance, multivariate linear regression was performed to remove age and sex covariates. Scikit-learn's "PowerTransformer" function was

used to stabilize variance and minimize skewness in order to normalize the EC features (<https://scikit-learn.org/stable/>)^[56,32].

The multivariate linear regression was used to reduce the influences of age and sex on the features⁵⁷.

The multivariate linear regression function can be defined as the following formula:

$$\text{Feature}_{(i,j)} = \beta_{(i,j)}^0 + \beta_i^{\text{age}} * \text{age}_j + \beta_i^{\text{sex}} * \text{sex}_j \quad (1)$$

where $i \in \{1, \dots, N\}$ is the feature index, $j \in \{1, \dots, M\}$ is the participant index. $\beta_{(i,j)}^0$ is the feature value of the j th participant after removing the age and sex covariates. age_j and sex_j represent the age and sex of the j th participant, respectively. β_i^{age} and β_i^{sex} represent the age and sex regression coefficients of the i th model, respectively.

The entire EC extraction procedure is shown in [Figure 2](#).

Figure 2. The entire EC extraction flow chart. ROI: region of interest.

Feature selection and classification model. Because the number of extracted features is much higher than the number of samples, feature selection is needed to reduce the dimension of the features. The feature selection and classification models used here are similar to those used in our previous study on classifying depression and extracting biomarkers using FC and network attributes⁸. We first used a two-sample t-test to select features with P-values less than 0.05, and to prevent information leakage, this step was only performed on the training set. This two-sample t-test can greatly compress the feature dimension and eliminate a large number of invalid features^[58,59]. Then, we used LightGBM²⁷ and SVM-RFECV implemented by Scikit-learn³² to respectively select important features. Both of them are model-based feature selection methods that are often used to select important features^[60,61], and these feature selection methods have achieved good results in classifying MDD using FC⁸.

Feature selection and classification method steps. As using a model-based feature selection method, we have integrated the procedures of feature selection and classification. It means that we also used a machine learning model in the feature selection procedure. The feature selection and classification method include two procedures: feature selection and construction of the classification model. We

employed a nested five-fold cross-validation strategy during both the feature selection and classification procedures. The folds in the inner loop were used to tune the hyperparameters of the models. The outer folds were used to extract the important features and evaluate the classification performance, respectively. The detailed steps of the method are as follows:

Procedure 1: Feature selection.

Because the dimension of the extracted features is very high, we need to select the features that contribute greatly to the classification model. (The reason why dimensionality reduction methods such as PCA⁶² were not used is that we hope to identify which features contribute greatly when the model achieves the best classification performance, and then the features that contribute greatly to the model can be regarded as the EC of MDD that have changed). The steps of the feature selection procedure are as follows:

1. The data set is partitioned into a training set and a test set using an outer loop of a five-fold cross-validation strategy.

Repeat steps 2 to 7 for each partitioned dataset.

2. A two-sample t-test with a p-value less than 0.05 was used to filter out the screened EC in the training set. (The features in the test set were set to be the same as those in the training set.)

3. In the training set (performing an inner loop of five-fold cross-validation), the best hyperparameters of the feature selection model (LinearSVM/LightGBM) using the features screened out by the two-sample t-test were obtained using the hyperparameter optimization algorithm of Optuna⁶³.

4. In the training set, the imbalanced-learn's synthetic minority oversampling technique^[64,65] is used to maintain a balance in the sample proportion so that the ratio of MDDs to HCs is close to 1:1 (The test set is not oversampled).

5. The oversampled training set is used to train the feature selection model (LinearSVM/LightGBM) with the best hyperparameters.

6. The test set is used to test the performance of the models. The test results are saved for comparison with the classification model retrained with important features later.

7. In the training set, SVM-RFECV is used to obtain an important feature subset for the LinearSVM model; the "feature_importance_" function is used to select important features for the LightGBM model, which is another important feature subset.

8. When the outer loop of five-fold cross-validation is complete, there are five important feature subsets for the LinearSVM and LightGBM models, respectively. The intersections of the five feature subsets are used as the final features.

[Figure 3](#) shows the steps of the important feature subsets extraction procedure.

Figure 3. The flow chart for the extraction of important feature subsets.

Procedure 2: Classification model training and testing.

1. The data set is partitioned into a training set and a test set using an outer loop of a five-fold cross-validation strategy.

Repeat steps 2 to 3 for each partitioned dataset.

2. In the training set (performing an inner loop of five-fold cross-validation), the best hyperparameters of the classification model (LinearSVM/LightGBM) using the final features selected by Procedure 1 (Feature selection) were obtained using the hyperparameter optimization algorithm of Optuna⁶³.

3. The test set is used to test different models and obtain testing results.

4. The model with the best performance is selected as the model used for MDD classification.

Procedure 3: Contribution analysis of the selected features

1. Selecting the classification model from step2 (Classification model training and testing).

2. In the outer loop of the five-fold cross-validation, SHAP was used to analyze the contribution of each feature to each classification model.

Hyperparameter setting. The feature selection and classification model involve many hyperparameters. For feature selection, we first performed a two-sample t-test on all features, retaining features with p-values below 0.05. Model-based feature selection methods were then used. The "sklearn.feature_selection.RFECV" function was used for feature selection, which was set to

remove ten percent of unimportant features at each iteration, "scoring" was set to "balanced_accuracy," "cv" was set to "RepeatedStratifiedKFold (n_splits=5, n_repeats=1)." LightGBM used the "feature_importances_" function for feature selection, and the "importance_type" parameter was set to the default option "split," retaining features with "feature_importances_" values greater than or equal to 1.

For the classification model, we used Optuna to perform a hyperparameter search for the hyperparameters of the classification model. We did five-fold cross-validation on the training set, using the accuracy of the five-fold cross-validation on the training set as the target for Optuna tuning optimization.

We set the Optuna tuning iterations to 100 ("n_trials" was set to 100) and limited the time to 10 minutes ("timeout" was set to 600 seconds) for LinearSVM and LightGBM. (LinearSVM's "max_iter" was set to ten million.). The detailed search space for the hyperparameters of LinearSVM is shown in Supplementary Material (see Supplementary Table S3), while the detailed search space for the hyperparameters of LightGBM is shown in Supplementary Material (see Supplementary Table S5).

Conflict of Interest

All authors declare no conflict of interest.

References

1. Segal, D. L. (2010). Diagnostic and statistical manual of mental disorders (DSM-IV-TR). The Corsini Encyclopedia of Psychology, 1-3. <https://doi.org/10.1002/9780470479216.corpsy0271>
2. World Health Organization, (1992). International Classification of Mental and Behavioural Disorders (ICD-10). Geneva: WHO.
3. Hamilton, M. (1960). A rating scale for depression. Journal of neurology, neurosurgery, and psychiatry, 23(1), 56. <https://doi.org/10.1136/jnnp.23.1.56>
4. Bordini, B. J., Stephany, A., & Kliegman, R. (2017). Overcoming diagnostic errors in medical practice. The Journal of pediatrics, 185, 19-25. <https://doi.org/10.1016/j.jpeds.2017.02.065>
5. Sen, B., Mueller, B., Klimes-Dougan, B., Cullen, K., & Parhi, K. K. (2019, July). Classification of major depressive disorder from resting-state fMRI. In 2019 41st Annual International Conference of the IEEE Engineering in Medicine and Biology Society (EMBC) (pp. 3511-3514). IEEE. <https://doi.org/10.1109/EMBC.2019.8856453>

6. Sen, B., Cullen, K. R., & Parhi, K. K. (2020). Classification of adolescent major depressive disorder via static and dynamic connectivity. *IEEE Journal of Biomedical and Health Informatics*, 25(7), 2604-2614. <https://doi.org/10.1109/JBHI.2020.3043427>
7. Peng, X., Wu, X., Gong, R., Yang, R., Wang, X., Zhu, W., & Lin, P. (2021). Sub-regional anterior cingulate cortex functional connectivity revealed default network subsystem dysfunction in patients with major depressive disorder. *Psychological Medicine*, 51(10), 1687-1695. <https://doi.org/10.1017/S0033291720000434>
8. Dai, P., Xiong, T., Zhou, X., Ou, Y., Li, Y., Kui, X., ... & Rest-Meta-Mdd Consortium. (2022). The alterations of brain functional connectivity networks in major depressive disorder detected by machine learning through multisite rs-fMRI data. *Behavioural Brain Research*, 435, 114058. <https://doi.org/10.1016/j.bbr.2022.114058>
9. Zhang, J., Kucyi, A., Raya, J., Nielsen, A. N., Nomi, J. S., Damoiseaux, J. S., ... & Whitfield-Gabrieli, S. (2021). What have we really learned from functional connectivity in clinical populations?. *NeuroImage*, 242, 118466. <https://doi.org/10.1016/j.neuroimage.2021.118466>
10. Yang, X., Zhang, N., & Schrader, P. (2022). A study of brain networks for autism spectrum disorder classification using resting-state functional connectivity. *Machine Learning with Applications*, 8, 100290. <https://doi.org/10.1016/j.mlwa.2022.100290>
11. RaviPrakash, H., Watane, A., Jambawalikar, S., & Bagci, U. (2019). Deep learning for functional brain connectivity: are we there yet?. *Deep Learning and Convolutional Neural Networks for Medical Imaging and Clinical Informatics*, 347-365. https://doi.org/10.1007/978-3-030-13969-8_17
12. Nakano, T., Takamura, M., Ichikawa, N., Okada, G., Okamoto, Y., Yamada, M., ... & Yoshimoto, J. (2020). Enhancing multi-center generalization of machine learning-based depression diagnosis from resting-state fMRI. *Frontiers in Psychiatry*, 11, 400. <https://doi.org/10.3389/fpsyg.2020.00400>
13. Chun, J. Y., Sendi, M. S., Sui, J., Zhi, D., & Calhoun, V. D. (2020, July). Visualizing Functional Network Connectivity Difference between Healthy Control and Major Depressive Disorder Using an Explainable Machine-learning Method. In 2020 42nd Annual International Conference of the IEEE Engineering in Medicine & Biology Society (EMBC) (pp. 1424-1427). IEEE. <https://doi.org/10.1109/EMBC44109.2020.9175685>
14. Yamashita, A., Sakai, Y., Yamada, T., Yahata, N., Kunimatsu, A., Okada, N., ... & Imamizu, H. (2020). Generalizable brain network markers of major depressive disorder across multiple imaging sites. *PLoS biology*, 18(12), e3000966. <https://doi.org/10.1371/journal.pbio.3000966>
15. Shi, Y., Zhang, L., Wang, Z., Lu, X., Wang, T., Zhou, D., & Zhang, Z. (2021). Multivariate machine learning analyses in identification of major depressive disorder using resting-state functional connectivity: A multicentral study. *ACS Chemical Neuroscience*, 12(15), 2878-2886. <https://doi.org/10.1021/acschemneuro.1c00256>
16. Friston, K. J. (1994). Functional and effective connectivity in neuroimaging: a synthesis. *Human brain mapping*, 2(1-2), 56-78. <https://doi.org/10.1002/hbm.460020107>
17. Granger, C. W. (1969). Investigating causal relations by econometric models and cross-spectral methods. *Econometrica: journal of the Econometric Society*, 424-438. <https://doi.org/10.2307/1912791>
18. Zang, Z. X., Yan, C. G., Dong, Z. Y., Huang, J., & Zang, Y. F. (2012). Granger causality analysis implementation on MATLAB: a graphic user interface toolkit for fMRI data processing. *Journal of neuroscience methods*, 203(2), 418-426. <https://doi.org/10.1016/j.jneumeth.2011.10.006>
19. Luo, L., Wu, H., Xu, J., Chen, F., Wu, F., Wang, C., & Wang, J. (2021). Abnormal large-scale resting-state functional networks in drug-free major depressive disorder. *Brain imaging and behavior*, 15(1), 96-106. <https://doi.org/10.1007/s11682-019-00236-y>
20. Gao, J., Li, Y., Wei, Q., Li, X., Wang, K., Tian, Y., & Wang, J. (2021). Habenula and left angular gyrus circuit contributes to response of electroconvulsive therapy in major depressive disorder. *Brain Imaging and Behavior*, 15(5), 2246-2253. <https://doi.org/10.1007/s11682-020-00418-z>
21. Guan, M., Wang, Z., Shi, Y., Xie, Y., Ma, Z., Liu, Z., ... & Wang, H. (2022). Altered Brain Function and Causal Connectivity Induced by Repetitive Transcranial Magnetic Stimulation Treatment for Major Depressive Disorder. *Frontiers in Neuroscience*, 16. <https://doi.org/10.3389/fnins.2022.855483>
22. Liu, J., Xu, P., Zhang, J., Jiang, N., Li, X., & Luo, Y. (2019). Ventral attention-network effective connectivity

predicts individual differences in adolescent depression. *Journal of Affective Disorders*, 252, 55-59. <https://doi.org/10.1016/j.jad.2019.04.033>

23. Rolls, E. T., Cheng, W., Gilson, M., Qiu, J., Hu, Z., Ruan, H., ... & Feng, J. (2018). Effective connectivity in depression. *Biological Psychiatry: Cognitive Neuroscience and Neuroimaging*, 3(2), 187-197. <https://doi.org/10.1016/j.bpsc.2017.10.004>
24. Dai, P., Zhou, X., Xiong, T., Ou, Y., Chen, Z., Zou, B., ... & Huang, Z. (2022). Altered Effective Connectivity Among the Cerebellum and Cerebrum in Patients with Major Depressive Disorder Using Multisite Resting-State fMRI. *The Cerebellum*, 1-9. <https://doi.org/10.1007/s12311-022-01454-9>
25. Wang, Y., Chen, X., Liu, R., Zhang, Z., Zhou, J., Feng, Y., ... & Zhou, Y. (2022). Disrupted effective connectivity of the default, salience and dorsal attention networks in major depressive disorder: a study using spectral dynamic causal modelling of resting-state fMRI. *Journal of Psychiatry and Neuroscience*, 47(6), E421-E434. <https://doi.org/10.1503/jpn.220038>
26. Geng, X., Xu, J., Liu, B., & Shi, Y. (2018). Multivariate classification of major depressive disorder using the effective connectivity and functional connectivity. *Frontiers in neuroscience*, 12, 38. <https://doi.org/10.3389/fnins.2018.00038>
27. Ke, G., Meng, Q., Finley, T., Wang, T., Chen, W., Ma, W., ... & Liu, T. Y. (2017). LightGBM: A highly efficient gradient boosting decision tree. *Advances in neural information processing systems*, 30. <https://dl.acm.org/doi/10.5555/3294996.3295074>
28. Chen, T., & Guestrin, C. (2016, August). Xgboost: A scalable tree boosting system. In *Proceedings of the 22nd ACM SIGKDD international conference on knowledge discovery and data mining* (pp. 785-794). <https://doi.org/10.1145/2939672.2939785>
29. Qin, K., Lei, D., Pinaya, W. H., Pan, N., Li, W., Zhu, Z., ... & Gong, Q. (2022). Using graph convolutional network to characterize individuals with major depressive disorder across multiple imaging sites. *EBioMedicine*, 78, 103977. <https://doi.org/10.1016/j.ebiom.2022.103977>
30. Kawahara, J., Brown, C. J., Miller, S. P., Booth, B. G., Chau, V., Grunau, R. E., ... & Hamarneh, G. (2017). BrainNetCNN: Convolutional neural networks for brain networks; towards predicting neurodevelopment. *NeuroImage*, 146, 1038-1049. <https://doi.org/10.1016/j.neuroimage.2016.09.046>
31. Zerveas, G., Jayaraman, S., Patel, D., Bhamidipaty, A., & Eickhoff, C. (2021, August). A transformer-based framework for multivariate time series representation learning. In *Proceedings of the 27th ACM SIGKDD Conference on Knowledge Discovery & Data Mining* (pp. 2114-2124). <https://doi.org/10.1145/3447548.3467401>
32. Pedregosa, F., Varoquaux, G., Gramfort, A., Michel, V., Thirion, B., Grisel, O., ... & Duchesnay, E. (2011). Scikit-learn: Machine learning in Python. *the Journal of machine Learning research*, 12, 2825-2830. <https://dl.acm.org/doi/10.5555/1953048.2078195>
33. Chen, S., Zhang, X., Lin, S., Zhang, Y., Xu, Z., Li, Y., ... & Qiu, Y. (2022). Suicide risk stratification among major depressed patients based on a machine learning approach and whole-brain functional connectivity. *Journal of affective disorders*. <https://doi.org/10.1016/j.jad.2022.11.022>
34. Dosenbach, N. U., Nardos, B., Cohen, A. L., Fair, D. A., Power, J. D., Church, J. A., ... & Schlaggar, B. L. (2010). Prediction of individual brain maturity using fMRI. *Science*, 329(5997), 1358-1361. <https://doi.org/10.1126/science.1194144>
35. Glasser, M. F., Coalson, T. S., Robinson, E. C., Hacker, C. D., Harwell, J., Yacoub, E., ... & Van Essen, D. C. (2016). A multi-modal parcellation of human cerebral cortex. *Nature*, 536(7615), 171-178. <https://doi.org/10.1038/nature18933>
36. R. S. Desikan, F. Ségonne et al., "An automated labeling system for subdividing the human cerebral cortex on MRI scans into gyral based regions of interest", *Neuroimage*, vol. 31, no. 3, pp. 968-980, 2006. <https://doi.org/10.1016/j.neuroimage.2006.01.021>
37. Fan, L., Li, H., Zhuo, J., Zhang, Y., Wang, J., Chen, L., ... & Jiang, T. (2016). The human brainnetome atlas: a new brain atlas based on connectional architecture. *Cerebral cortex*, 26(8), 3508-3526. <https://doi.org/10.1093/cercor/bhw157>
38. Xu, Z., Gao, C., Tan, T., Jiang, W., Wang, T., Chen, Z., ... & Yuan, Y. (2022). Combined HTR1A/1B methylation and human functional connectome to recognize patients with MDD. *Psychiatry Research*, 317, 114842. <https://doi.org/10.1016/j.psychres.2022.114842>

39. Xia, M., Wang, J., & He, Y. (2013). BrainNet Viewer: a network visualization tool for human brain connectomics. *PLoS one*, 8(7), e68910. <https://doi.org/10.1371/journal.pone.0068910>

40. Betzel, R. F., Byrge, L., He, Y., Goñi, J., Zuo, X. N., & Sporns, O. (2014). Changes in structural and functional connectivity among resting-state networks across the human lifespan. *Neuroimage*, 102, 345-357. <https://doi.org/10.1016/j.neuroimage.2014.07.067>

41. Nashiro, K., Sakaki, M., Braskie, M. N., & Mather, M. (2017). Resting-state networks associated with cognitive processing show more age-related decline than those associated with emotional processing. *Neurobiology of aging*, 54, 152-162. <https://doi.org/10.1016/j.neurobiolaging.2017.03.003>

42. Schmahmann, J. D. (2004). Disorders of the cerebellum: ataxia, dysmetria of thought, and the cerebellar cognitive affective syndrome. *The Journal of neuropsychiatry and clinical neurosciences*, 16(3), 367-378. <https://doi.org/10.1176/jnp.16.3.367>

43. Schmahmann, J. D. (2010). The role of the cerebellum in cognition and emotion: personal reflections since 1982 on the dysmetria of thought hypothesis, and its historical evolution from theory to therapy. *Neuropsychology review*, 20(3), 236-260. <https://doi.org/10.1007/s11065-010-9142-x>

44. Sun, J., Xu, L., Ma, Y., Guo, C., Du, Z., Gao, S., ... & Fang, J. (2022). Different characteristics of striatal resting-state functional connectivity in treatment-resistant and non-treatment-resistant depression. *Psychiatry Research: Neuroimaging*, 111567. <https://doi.org/10.1016/j.pscychresns.2022.111567>

45. Han, J. K., Kwon, S. H., Kim, Y. G., Choi, J., Kim, J. I., Lee, Y. S., ... & Kim, S. J. (2021). Ablation of STAT3 in Purkinje cells reorganizes cerebellar synaptic plasticity in long-term fear memory network. *Elife*, 10, e63291. <https://doi.org/10.7554/elife.63291>

46. Adamaszek, M., D'Agata, F., Ferrucci, R. et al. Consensus Paper: Cerebellum and Emotion. *Cerebellum* 16, 552–576 (2017). <https://doi.org/10.1007/s12311-016-0815-8>

47. van Dun, K., Manto, M., & Meesen, R. (2022). Cerebellum and neurorehabilitation in emotion with a focus on neuromodulation. In *The Emotional Cerebellum* (pp. 285-299). Springer, Cham. https://doi.org/10.1007/978-3-030-99550-8_18

48. Lupo, M., Olivito, G., Siciliano, L., Masciullo, M., Bozzali, M., Molinari, M., & Leggio, M. (2018). Development of a psychiatric disorder linked to cerebellar lesions. *The Cerebellum*, 17(4), 438-446. <https://doi.org/10.1007/s12311-018-0926-5>

49. Yan, C. G., Chen, X., Li, L., Castellanos, F. X., Bai, T. J., Bo, Q. J., ... & Zang, Y. F. (2019). Reduced default mode network functional connectivity in patients with recurrent major depressive disorder. *Proceedings of the National Academy of Sciences*, 116(18), 9078-9083. <https://doi.org/10.1073/pnas.1900390116>

50. Yan, C., & Zang, Y. (2010). DPARSF: a MATLAB toolbox for " pipeline" data analysis of resting-state fMRI. *Frontiers in systems neuroscience*, 4, 13. <https://doi.org/10.3389/fnsys.2010.00013>

51. Friston, K. J., Williams, S., Howard, R., Frackowiak, R. S., & Turner, R. (1996). Movement-related effects in fMRI time-series. *Magnetic resonance in medicine in medicine*, 35(3), 346-355. <https://doi.org/10.1002/mrm.191002030312>

52. Tzouriomazoyer, N., Landeau, B., Papathanassiou, D., Crivello, F., Etard, O., Delcroix, N., et al. (2002). Automated anatomical labeling of activations in SPM using a macroscopic anatomical parcellation of the MNI MRI single-subject. *Neuroimage* 15, 273–289. <https://doi.org/10.1006/nimg.2001.0978>

53. Yu, M., Linn, K. A., Cook, P. A., Phillips, M. L., McInnis, M., Fava, M., ... & Sheline, Y. I. (2018). Statistical harmonization corrects site effects in functional connectivity measurements from multi-site fMRI data. *Human brain mapping*, 39(11), 4213-4227. <https://doi.org/10.1002/hbm.24241>

54. Fortin, J. P., Cullen, N., Sheline, Y. I., Taylor, W. D., Aselcioglu, I., Cook, P. A., ... & Shinohara, R. T. (2018). Harmonization of cortical thickness measurements across scanners and sites. *Neuroimage*, 167, 104-120. <https://doi.org/10.1016/j.neuroimage.2017.11.024>

55. Johnson, W. E., Li, C., & Rabinovic, A. (2007). Adjusting batch effects in microarray expression data using empirical Bayes methods. *Biostatistics*, 8(1), 118-127. <https://doi.org/10.1093/biostatistics/kxj037>

56. Yeo, I. K., & Johnson, R. A. (2000). A new family of power transformations to improve normality or symmetry. *Biometrika*, 87(4), 954-959. <https://doi.org/10.1093/biomet/87.4.954>

57. Zhang, C., Cahill, N. D., Arbabshirani, M. R., White, T., Baum, S. A., & Michael, A. M. (2016). Sex and age

effects of functional connectivity in early adulthood. *Brain connectivity*, 6(9), 700-713. <https://doi.org/10.1089/brain.2016.0429>

- 58. Wang, L., Zhu, Y., Wu, L., Zhuang, Y., Zeng, J., & Zhou, F. (2022). Classification of Chemotherapy-Related Subjective Cognitive Complaints in Breast Cancer Using Brain Functional Connectivity and Activity: A Machine Learning Analysis. *Journal of Clinical Medicine*, 11(8), 2267. <https://doi.org/10.3390/jcm11082267>
- 59. Tong, Y., Huang, X., Qi, C. X., & Shen, Y. (2021). Altered functional connectivity of the primary visual cortex in patients with iridocyclitis and assessment of its predictive value using machine learning. *Frontiers in Immunology*, 12, 660554. <https://doi.org/10.3389/fimmu.2021.660554>
- 60. Luo, Q., Liu, W., Jin, L., Chang, C., & Peng, Z. (2021). Classification of Obsessive-Compulsive Disorder Using Distance Correlation on Resting-State Functional MRI Images. *Frontiers in Neuroinformatics*, 15. <https://doi.org/10.3389/fninf.2021.676491>
- 61. Han, L., Yang, T., Pu, X., Sun, L., Yu, B., & Xi, J. (2021). Alzheimer's Disease Classification using LightGBM and Euclidean Distance Map. 2021 IEEE 5th Advanced Information Technology, Electronic and Automation Control Conference (IAEAC), 5, 1540-1544. <https://doi.org/10.1109/IAEAC50856.2021.9391046>
- 62. Abdi, H., & Williams, L. J. (2010). Principal component analysis. *Wiley interdisciplinary reviews: computational statistics*, 2(4), 433-459. <https://doi.org/10.1002/wics.101>
- 63. Akiba, T., Sano, S., Yanase, T., Ohta, T., & Koyama, M. (2019, July). Optuna: A next-generation hyperparameter optimization framework. In *Proceedings of the 25th ACM SIGKDD international conference on knowledge discovery & data mining* (pp. 2623-2631). <https://doi.org/10.1145/3292500.3330701>
- 64. Lemaître, G., Nogueira, F., & Aridas, C. K. (2017). Imbalanced-learn: A python toolbox to tackle the curse of imbalanced datasets in machine learning. *The Journal of Machine Learning Research*, 18(1), 559-563. <https://dl.acm.org/doi/10.5555/3122009.3122026>
- 65. Han, H., Wang, W. Y., & Mao, B. H. (2005, August). Borderline-SMOTE: a new over-sampling method in imbalanced data sets learning. In *International conference on intelligent computing* (pp. 878-887). Springer, Berlin, Heidelberg. https://dl.acm.org/doi/10.1007/11538059_91

Figures and Tables

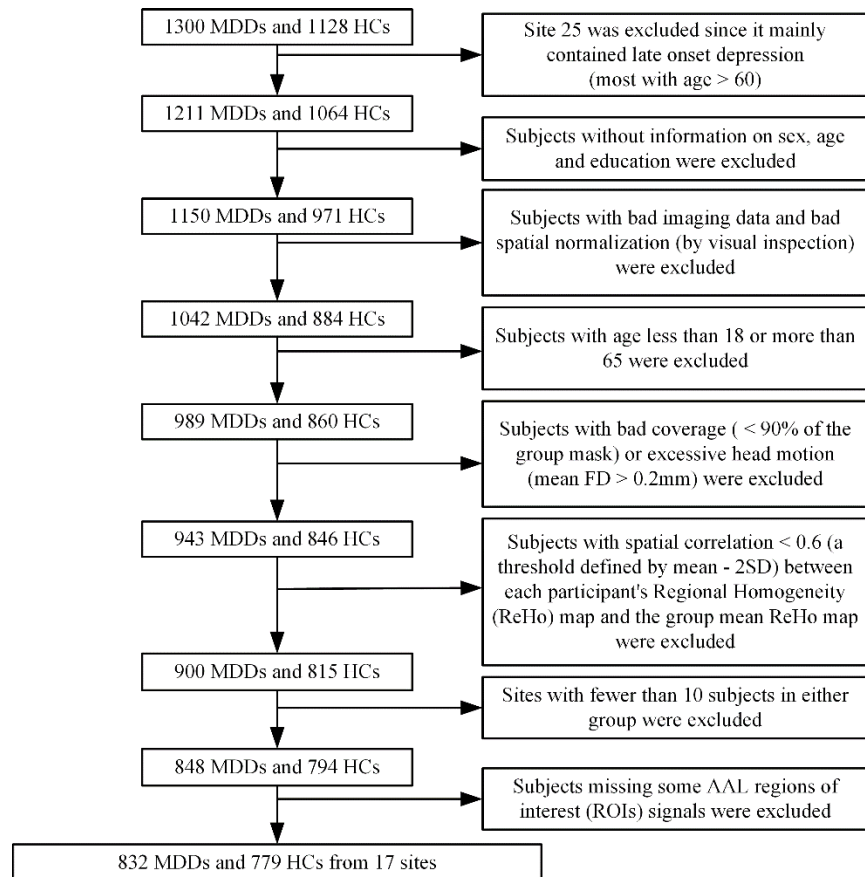


Figure 1. Sample screening procedure.

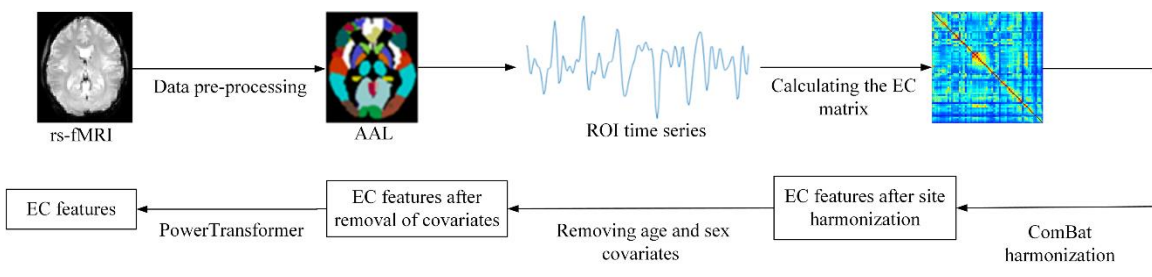


Figure 2. The entire EC extraction flow chart. ROI: region of interest.

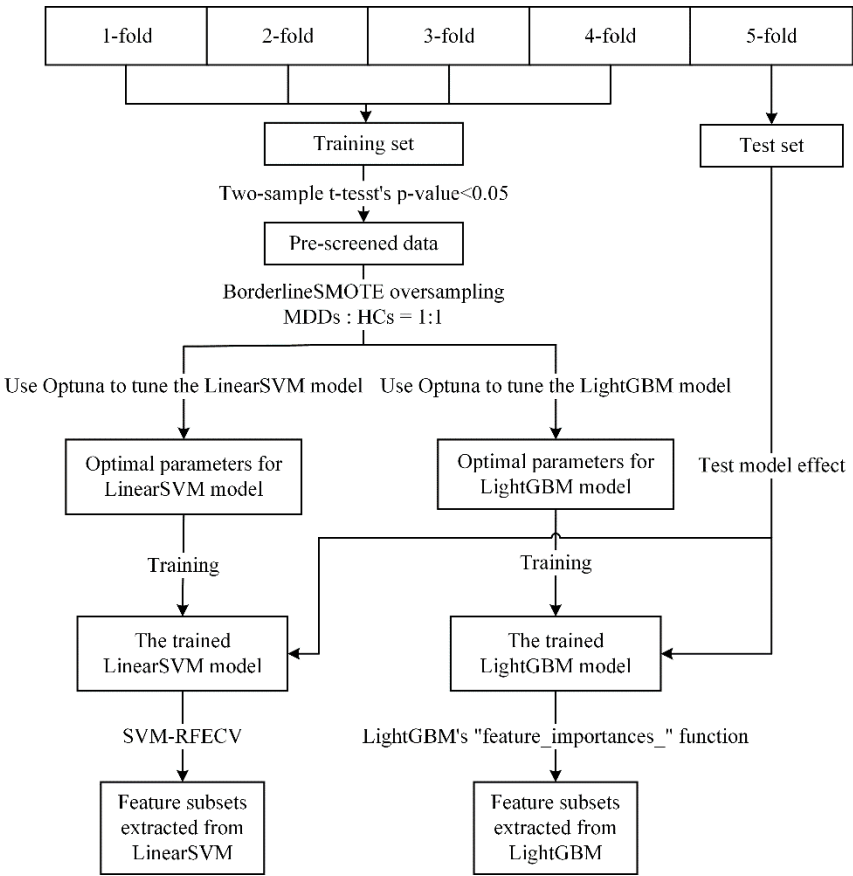


Figure 3. The flow chart for the extraction of important feature subset.

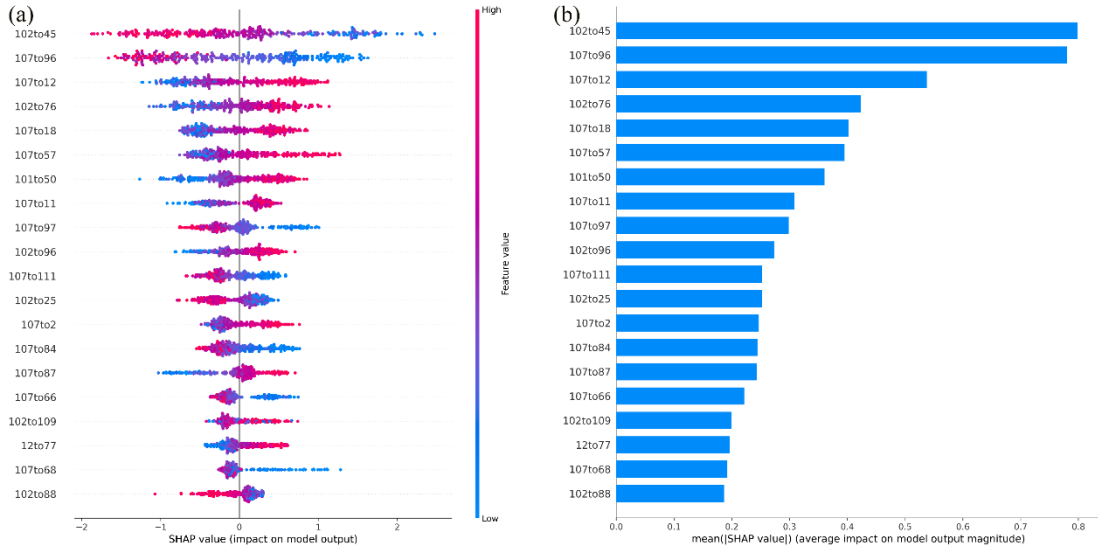


Figure 4. Analysis of the contribution of important features. The labels on the left side of the vertical axis in (a) and (b) of this Figure indicate different features. In Figure (a), the horizontal axis is the SHAP value coordinate axis, and the zero point of the coordinate is the dividing point to judge whether the sample is a healthy person or a patient with MDD. A SHAP value less than zero indicates that the sample is classified as an HC, and a SHAP value greater than zero indicates that the sample is classified as a patient with MDD. Each row of the graph represents a feature, from top to bottom, according to the importance of the feature. Each point on a certain important feature represents a sample's SHAP value, and the point's color depth represents the feature value's size. From this Figure, we can see the contribution of the features to the classification model. Figure (b) shows the mean ($|SHAP\ value|$) of each selected feature. The larger the mean ($|SHAP\ value|$), the higher the contribution of this feature to the model classification, and the more important it is. The number of the feature name in the Figure represents the ROI number of the AAL atlas. 102to45: EC of Cerebellum_7b_R and Cuneus_L; 107to96: EC of Cerebellum_10_L and Cerebellum_3_R; 107to12: EC of Cerebellum_10_L and Frontal_Inf_Oper_R; 102to76: EC of Cerebellum_7b_R and Pallidum_R; 107to18: EC of Cerebellum_10_L and Rolandic_Oper_R; 107to57: EC of Cerebellum_10_L and Postcentral_L; 101to50: EC of Cerebellum_7b_L and Occipital_Sup_R; 107to11: EC of Cerebellum_10_L and Frontal_Inf_Oper_L; 107to97: EC of Cerebellum_10_L and Cerebellum_4_5_L; 102to96: EC of Cerebellum_7b_R and Cerebellum_3_R; 107to111: EC of Cerebellum_10_L and Vermis_4_5; 102to25: EC of Cerebellum_7b_R and Frontal_Med_Orb_L; 107to2: EC of Cerebellum_10_L and Precentral_R; 107to84: EC of Cerebellum_10_L and Temporal_Pole_Sup_R; 107to87: EC of Cerebellum_10_L and Temporal_Pole_Mid_L; 107to66: EC of Cerebellum_10_L and Angular_R; 102to109: EC of Cerebellum_7b_R and Vermis_1_2; 12to77: EC of Frontal_Inf_Oper_R and Thalamus_L; 107to68: EC of Cerebellum_10_L and Precuneus_R; 102to88: EC of Cerebellum_7b_R and Temporal_Pole_Mid_R.

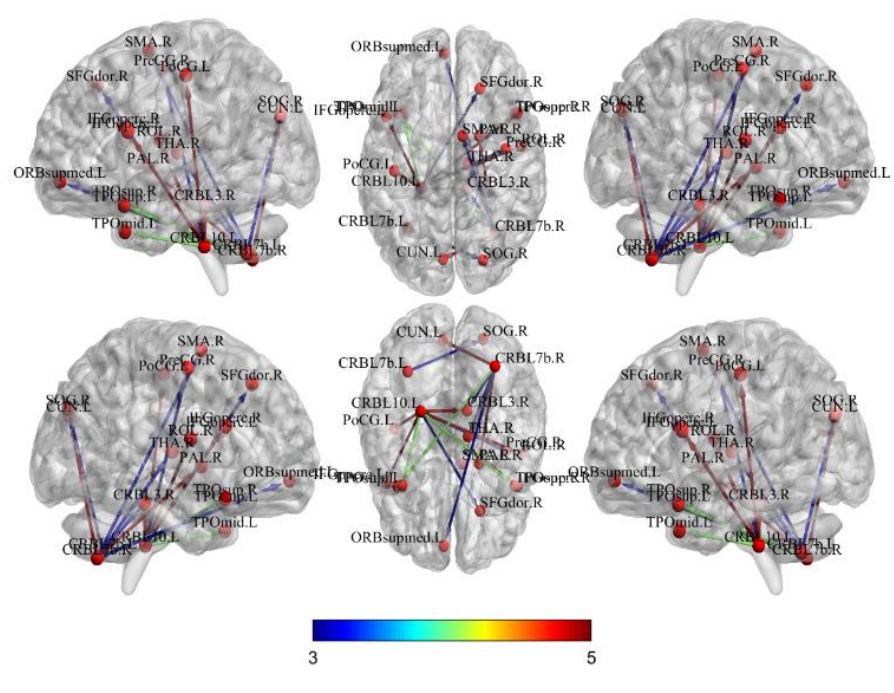


Figure 5. Brain visualization of high-contributing EC. The horizontal axis represents the number of occurrences of EC features in the five subsets of high-contributing EC features. PreCG.R: Precentral_R; SFGdor.R: Frontal_Sup_R; IFGoperc.L: Frontal_Inf_Oper_L; IFGoperc.R: Frontal_Inf_Oper_R; ROL.R: Rolandic_Oper_R; SMA.R: Supp_Motor_Area_R; ORBsupmed.L: Frontal_Med_Orb_L; CUN.L: Cuneus_L; SOG.R: Occipital_Sup_R; PoCG.L: Postcentral_L; PAL.R: Pallidum_R; THA.R: Thalamus_R; TPOsup.L: Temporal_Pole_Sup_L; TPOsup.R: Temporal_Pole_Sup_R; TPOmid.L: Temporal_Pole_Mid_L; CRBL3.R: Cerebellum_3_R; CRBL7b.L: Cerebellum_7b_L; CRBL7b.R: Cerebellum_7b_R; CRBL10.L: Cerebellum_10_L.

Table 1. The comparison of the classification performance of machine learning and deep learning models.

Model	Accuracy (%)	Sensitivity (%)	Specificity (%)
Rbf-SVM-FC	64.87%	66.71%	62.89%
Rbf-SVM-EC	83.30%	84.62%	81.90%
Random Forest-FC	62.33%	62.86%	61.74%
Random Forest-EC	89.39%	88.70%	90.11%
XGBoost-FC	62.88%	64.06%	61.62%
XGBoost-EC	91.74%	91.10%	92.42%
GCN-FC	60.42%	66.32%	57.34%
GCN-EC	82.26%	81.84%	83.16%
BrainNetCNN-FC	62.15%	66.81%	57.18%
BrainNetCNN-EC	91.18%	90.36%	92.05%
Transformer-FC	62.66%	64.75%	60.42%
Transformer-EC	86.73%	83.96%	89.71%
LightGBM-FC	65.24%	66.59%	63.79%
LightGBM-EC	92.43%	91.47%	93.45%

Table 2. The classification performance of two classifiers before and after feature selection.

Models	Features before feature selection				Features after feature selection			
	Number of features	Accuracy	Sensitivity	Specificity	Number of features	Accuracy	Sensitivity	Specificity
LinearSVM	13340	77.15%	77.76%	76.50%	97	86.84%	87.51%	86.14%
LightGBM	13340	92.43%	91.47%	93.45%	97	94.35%	93.52%	95.25%

Notes: Feature selection was performed using a two-sample t-test and LightGBM's "feature_importances_" function.

Table 3. The results of migration experiments with highly discriminatory EC.

Models	The REST-meta-MDD Consortium			The DecNef Project Brain Data Repository				
	Number of features	Accuracy	Sensitivity	Specificity	Number of features	Accuracy	Sensitivity	Specificity
LinearSVM	97	86.84%	87.51%	86.14%	97	83.57%	85.49%	82.63%
LightGBM	97	94.35%	93.52%	95.25%	97	94.74%	90.59%	96.75%

Notes: Feature selection was performed using a two-sample t-test and LightGBM's "feature_importances_" function.

Table 4. The comparison of recent research results on classifying MDD using FC or EC features.

Literature	Size of sample	Feature	Classifier	Accuracy	Sensitivity	Specificity
Dai et al. ⁸	832 MDDs : 779 HCs	FC between 116 ROIs (the AAL atlas, including the cerebellum); network attribute features extracted from FC	LinearSVM, LightGBM	68.90%	71.75%	65.84%
Chen et al. ³³	162 MDDs : 38 HCs	FC between 142 ROIs (the Dosenbach atlas ³⁴ , excluding the cerebellum)	SVM	88.50%	80.86%	92.76%
Shi et al. ¹⁵	1021 MDDs : 1100 HCs	FC between 90 ROIs (the AAL atlas, excluding the cerebellum)	XGBoost	72.80%	72.00%	73.90%
Yamashita et al. ¹⁴	385 MDDs : 849 HCs	FC between 379 ROIs (the Glasser's 379 surface-based parcellations ³⁵)	SVM	68.00%	62.00%	73.00%
Sen et al. ⁵	49 MDDs : 33 HCs	FC between 85 ROIs (the freesurfer cortical parcel-lation atlas ³⁶) ; network attribute features extracted from FC	LinearSVM	79.00%	86.00%	70.00%
Geng et al. ²⁶	24 MDDs : 24 HCs	FC and EC 272 ROIs (including the AAL atlas and Brainnetome atlas ³⁷)	Non-LinearSVM, LinearSVM, k-Nearest Neighbor (KNN) and Logistic Regression (LR)	91.67%	88.00%	88.00%
Xu et al. ³⁸	98 MDDs : 63HCs	HTR1A/1B methylation+FC between 116 ROIs (the AAL atlas)	Random Forest	81.78%	92.01%	68.29%
Qin et al. ²⁹	821MDDs:765HCs	FC between 160 ROIs (the Dosenbach atlas ³⁴)	GCN	81.50%	83.40%	80.00%
Ours	832 MDDs : 779 HCs	EC between 116 ROIs (the AAL atlas, including the cerebellum);	LightGBM	94.35%	93.52%	95.25%

Notes: ROIs : regions of interest.

Table 5. High-contributing EC.

ROI-FROM	ROI-TO	Across the network	MDDs(avg)	HCs(avg)	P-value
Cerebellum_10_L	Rolandic_Oper_R	Yes	0.4677	-0.4995	<0.0001
Cerebellum_7b_R	Cuneus_L	Yes	-0.0920	0.0983	0.0001
Cerebellum_10_L	Frontal_Inf_Oper_L	Yes	0.4713	-0.5034	<0.0001
Cerebellum_10_L	Postcentral_L	Yes	0.3286	-0.3509	<0.0001
Cerebellum_10_L	Cerebellum_3_R	Yes	-0.4256	0.4546	<0.0001
Cerebellum_7b_R	Pallidum_R	Yes	0.1064	-0.1136	<0.0001
Cerebellum_10_L	Frontal_Inf_Oper_R	Yes	0.4785	-0.5110	<0.0001
Cerebellum_7b_R	Temporal_Pole_Sup_L	Yes	-0.1540	0.1645	<0.0001
Cerebellum_10_L	Temporal_Pole_Mid_L	Yes	0.2418	-0.2582	<0.0001
Cerebellum_10_L	Temporal_Pole_Sup_R	Yes	-0.3159	0.3374	<0.0001
Cerebellum_7b_R	Supp_Motor_Area_R	Yes	0.0909	-0.0971	0.0002
Cerebellum_10_L	Frontal_Sup_R	Yes	-0.4122	0.4403	<0.0001
Cerebellum_7b_R	Thalamus_R	Yes	0.1923	-0.2054	<0.0001
Cerebellum_10_L	Precentral_R	Yes	0.1501	-0.1603	<0.0001
Cerebellum_7b_R	Frontal_Med_Orb_L	Yes	-0.0980	0.1046	<0.0001
Cerebellum_7b_L	Occipital_Sup_R	Yes	0.0934	-0.0998	0.0001
Cerebellum_7b_R	Cerebellum_3_R	Yes	0.1134	-0.1211	<0.0001

Notes: Across the network refers to whether the two ROIs involved in the feature belong to the same resting-state network. MDDs (avg) and HCs (avg) refer to the average of the feature values (The feature values have been processed by age & sex covariate regression and ComBat.) of MDDs and HCs in the REST-meta-MDD Consortium dataset, respectively. P-value is the result of a two-sample t-test for feature values between MDDs and HCs in the REST-meta-MDD Consortium dataset.